Tellus
SERIES B
CHEMICAL
AND PHYSICAL
METEOROLOGY
PUBLISHED BY THE INTERNATIONAL METEOROLOGICAL INSTITUTE IN STOCKHOLM

Tellus (2011), 63B, 382–394

TELLUS

Characterization of new particle and secondary aerosol formation during summertime in Beijing, China

By Y. M. ZHANG[1,2], X. Y. ZHANG[1]*, J. Y. SUN[1], W. L. LIN[1], S. L. GONG[3], X. J. SHEN[1] and S. YANG[4], [1]*Key Laboratory for Atmospheric Chemistry, Centre for Atmosphere Watch and Services, Chinese Academy of Meteorological Sciences, China Meteorological Administration, 46 Zhongguancun S. Avenue, Beijing 100081, China;* [2]*Graduate University of Chinese Academy of Sciences, 19A Yuquanlu Shijingshan District, Beijing 100049, China;* [3]*Air Quality Research Division, Science and Technology Branch, Environment Canada 4905 Dufferin Street, Toronto, Ontario M3H 5T4, Canada;* [4]*State Key Laboratory of Numerical Modeling for Atmospheric Sciences and Geophysical Fluid Dynamics, Institute of Atmospheric Physics, CAS, Qijiahuozi Deshengmenwai, Beijing 100029, China*

(Manuscript received 27 May 2009; in final form 8 March 2011)

ABSTRACT

Size-resolved aerosol number and mass concentrations and the mixing ratios of O_3 and various trace gases were continuously measured at an urban station before and during the Beijing Olympic and Paralympic Games (5 June to 22 September, 2008). 23 new particle formation (NPF) events were identified; these usually were associated with changes in wind direction and/or rising concentrations of gas-phase precursors or after precipitation events. Most of the NPF events started in the morning and continued to noon as particles in the nucleation mode grew into the Aitken mode. From noon to midnight, the aerosols grew into the accumulation mode through condensation and coagulation. Ozone showed a gradual rise starting around 10:00 local time, reached its peak around 15:00 and then declined as the organics increased. The dominant new particle species were organics (40–75% of PM_1) and sulphate; nitrate and ammonium were more minor contributors.

1. Introduction

A better understanding of how secondary aerosol (SA) particles form is critical for developing more targeted pollution control measures and for more realistically parametrizing the distributions of sulphate, nitrate, ammonium and especially organic substances in aerosol models and related weather forecasting tools. New particle formation (NPF) and growth are a major source for ultra fine particles (UFP) in both clean and polluted atmospheres. NPF is also important for sustaining the ambient aerosol populations, not only in forested (Kulmala et al., 1998; Pirjola et al., 1998), coastal (O'Dowd et al., 1998; O'Dowd et al., 2002), rural/remote (Eisele and McMurry, 1997; Weber et al., 1999; Wiedensohler et al., 2002), arctic (Pirjola et al., 1998) and urban (Hämeri et al., 1996; Wiedensohler et al., 2002; Alam et al., 2003; Zhang et al., 2004a) areas, but also in mega cities such as Mexico City (Dunn et al., 2004), Beijing (Wehner et al., 2004) and New Delhi (Mönkkönen et al., 2005). Newly formed particles can grow into larger particles (>100 nm) in 1–2 d (Kulmala et al., 2004), and they may thus influence regional climate due to their effects on cloud formation, solar radiation and visibility. Given the health effects of fine particles (Oberdörster et al., 1995), including premature deaths and morbidity (Donaldson et al., 2002; Li et al., 2003), the abundance of these particles also is a human health concern (Zhang et al., 2004a).

The evolution of the particle number concentration and size spectra during nucleation events has been investigated in a number of field studies, often with techniques involving scanning mobility particle sizers (SMPSs; also known as DMPSs, differential mobility particle sizers) (Kulmala et al., 2001; Wiedensohler et al., 2002; Zhang et al., 2004a). In Beijing, there also have been several investigations into aerosol pollution and the mechanisms involved in aerosol formation (Wehner et al., 2004; Massling et al., 2008; Yue et al., 2010). However, comprehensive investigations into SA formation by simultaneously measuring fine particle number/mass-size distributions and the concentrations of aerosol precursor gases have not been conducted in Beijing, and this is the focus of the present study.

Here we present the results of an integrated field study in which we used a SMPS and an aerosol mass spectrometer (AMS) to evaluate changes in the particle number/mass-size distributions during the nucleation, condensation and coagulation of aerosol particles. Variations in the chemical composition of

*Corresponding author.
e-mail: xiaoye@cams.cma.gov.cn
DOI: 10.1111/j.1600-0889.2011.00533.x

size-resolved aerosol particles and the concentrations of their precursor gases also were documented. These measurements were conducted before and during the Beijing Olympic and Paralympic Games as part of the ground- and satellite-based monitoring campaign for Beijing and surrounding areas (Zhang et al., 2009). These coordinated studies were conducted to evaluate the effects of the restrictions on pollution emissions put into place during the games.

2. Experimental

2.1. Sampling and instrumentation

Selected atmospheric components were measured from 5 June to 22 September 2008 at an urban station in Beijing [the China Meteorological Administration (CMA) station, a 9-story building, 35 m above ground, 116°19.395′ E; 39° 56.916′ N]. Ambient air was sampled 1.5 m above the roof of the building through a 12.7 mm stainless steel tube (about 6 m long) and 1-m-long silicone conductive tube. Coarse particles were removed using an inline cyclone with a 2.5 μm cutoff (Model URG-2000-30EN, URG Corporation, Chapel Hill, NC, USA) that operated at a flow rate of 10 L min^{-1}.

A quadruple AMS (Aerodyne Research Inc. Boston, TX, USA) was deployed at the site and an SMPS (TSI 3936, TSI Asia Pacific Inc., Beijing, China) operated concurrently. Detailed descriptions of the AMS and its operation have been presented in Jayne et al. (2000) and Jimenez et al. (2003). Despite its comparatively large minimum-size cutoff (30–35 nm in vacuum aerodynamic diameter or 20 nm in physical diameter), the AMS is a useful tool for studying new particle growth events in the atmosphere because of its rapid response, high sensitivity and the simultaneous measurements of particle size distribution and chemical composition (Zhang et al., 2004a).

During the experiment, the AMS alternated between the particle time-of-flight (pToF) mode and the mass spectra (MS) mode every 15 s. Under the pToF mode operation, signals of 18 mass-to-charge ratios (m/z's) representative of NO_3^- (m/z 30 and 46), SO_4^{2-} (m/z 48, 64 and 98), organics (m/z 43, 44, 55, 57, 60, 77, 102 and 202), NH_4^+ (m/z 16,17), H_2O (m/z 18), and airbeam (N_2, m/z 28, O_2, m/z 32) were recorded as a function of particle size. Mass concentrations and size distributions were reported as 5-min averages.

The number concentrations of particles 12–550 nm in mobility diameter (D_m) were measured every 5 min using an SMPS system, which consisted of an Electrostatic Classifier controller platform (TSI Model 3080), a long differential mobility analyzer (DMA, TSI 3081) and a condensation particle counter (CPC, TSI 3010). The SMPS size distribution was constructed from the average of two scans (2.5 min each), which were taken at 5-min intervals. The sheath flow of the DMA was 4 L min^{-1}, and the DMA aerosol flow was set to 0.4 L min^{-1}. The fixed CPC flow rate was 1 L min^{-1}.

The AMS and SMPS were operated in parallel throughout the experiment. The particle sizes determined by the AMS were the vacuum aerodynamic diameters (D_{va}). The observed particle size distributions were classified into three modes according to the following convention: 'Nucleation mode' ($D_m \leq 25$ nm), 'Aitken mode' ($D_m = 25$–100 nm) and 'Accumulation mode' ($D_m = 100$–1000 nm). As the scanning size range of SMPS we used was 12–550 nm, the nucleation mode for that instrument was operationally defined as ranging from 12 to 25 nm.

Commercial instruments from Thermo Environmental Instruments, Inc. (Franklin, MA, USA) were used to continuously measure O_3 (TE 49C), $NO/NO_2/NO_X$ (TE 42 CTL), CO (TE 48C) and SO_2 (TE 43CTL). Daily zero/span checks and multipoint calibrations were done using a dynamic gas calibrator (TE 146C) in combination with a zero air supply (TE 111) and a set of standard reference gas mixtures (National Institute of Metrology, Beijing, China). For ozone, the standards were traceable to the standard reference photometer maintained by WMO World Calibration Centre in Switzerland (EMPA). More details for instrumentation and data process may be found in the papers by Lin et al. (2008) and Xu et al. (2008). Meteorological data such as atmospheric temperature, pressure, relative humidity (RH), precipitation, wind directions and wind speeds, also were collected at the sampling site.

Assuming that the formation and loss of the sulphur acid were in steady-state, the gas phase sulphuric acid proxy concentration was computed as follows:

$$[H_2SO_4\text{proxy}] = [SO_2] \cdot \text{SR}/\text{CS} \quad \text{(Kulmala et al., 2005)}, \quad (1)$$

where SR and CS are the global intensity of solar radiation and the condensational sink, respectively. CS describes the tendency for preexisting particles to remove condensable vapors from the atmosphere, and it was calculated according to the methods described by Kulmala et al. (2001), Kulmala et al. (2005), Dal Maso et al. (2002), Dal Maso et al. (2005) and Wu et al. (2007) as follows:

$$\text{CS} = 2\pi D \int_0^\infty D_p \beta_M(D_p) n(D_p) \mathrm{d}D_p = 2\pi D \sum_i \beta_M D_{p,i} N_i. \quad (2)$$

Here D is the diffusion coefficient, $n(D_p)$ represents the particle-size distribution function, and N_i is the particle number concentration in the i-th size fraction. In this study, particles ranging in size from12 nm to 550 nm were used to calculate the CS. β_M is the transitional correction factor for the mass flux (Kulmala et al., 1998)

The calibration schedule for the AMS during the study was as follows: electron multiplier gain (once 2–3 d), ionization efficiency (once a month) and particle sizing (once a month). Particle-free air (i.e. air filtered with a HEPA filter) was analysed using the same m/z's as during actual sampling to derive the detection limits (DLs) for the AMS measurements and for

quality control purposes. The calculated DLs for ammonium, sulphate, nitrate and organics were 0.018, 0.06, 0.012 and 0.03 $\mu g\,m^{-3}$, respectively, for 25-min averages. The DLs in this study are slightly higher than values previously reported (Sun et al., 2010); this is because the relatively long operating times used in this study increased the background noise.

A collection efficiency (CE) term was introduced to correct for the incomplete detection of aerosols by the AMS (Alfarra, 2004; Lanz et al., 2007); this was needed because a fraction of irregularly shaped particles may not reach the AMS vaporizer (Jayne et al., 2000; Tobias et al., 2000) and some bounce back of non-volatile particles may occur on the surface of vapourizer (Matthew et al., 2008). The CE is calibrated based on the ratio of the total AMS mass concentrations to the SMPS mass. For reasons discussed later, a fixed CE value of 1 was set for periods with high humidity except for June when it was set to 0.5. Generally good correlations between the reconstructed AMS and SMPS mass data were found [the aerosol density used in these calculations was assumed to be the average composition of $(NH_4)_2SO_4$, NH_4NO_3, NH_4Cl and organics, whose density is 1.8, 1.72 and 1.3 g cm^{-3}, respectively; see Figs 1a–d). The slopes of the fitted curves were 0.91, 1.1, 0.89 and 1.0 for June, July, August and September, respectively, with corresponding coefficients of determination (r^2) equal to 0.77, 0.83, 0.70 and 0.84.

Previous research has shown that the CE can be influenced by RH(Allan et al., 2004), particle acidity (Quinn et al., 2006), the particles' nitrate content (Crosier et al., 2007) and types of organic species present (Jimenez et al., 2003). In July 2008, a series of measures to control air pollution were implemented in Beijing, and during the Olympic Games and Paralympic Games, which were in August and September, additional special control measures were enacted. Those controls evidently resulted in lower organic aerosol and nitrate concentrations in association with weather conditions favourable for good air quality (Zhang et al., 2009). These large changes in aerosol composition, especially in nitrate and organics, were the reason for using different CEs for June compared with subsequent months. Moreover, we compared the AMS mass concentrations with those obtained with other instruments (a tapered element oscillating microbalance, Thermo Scientific, NY, USA, and a Grimm 180 laser spectroscopy particulate monitor, Grimm Aerosol Technik GmbH & Co., Ainring, Germany; data not shown), and the agreement in results indicates that the CE values used for the different months resulted in valid concentrations.

The concentrations of particle mass, organics, sulphate, nitrate and ammonium determined by AMS showed clear positive relationships with the OC, sulphate, nitrate and ammonium concentrations determined for 24-h $PM_{2.5}$ filter samples (Fig. 2). The latter were collected with a Minivol sampler (Airmatrics, USA) from 09:00 to 09:00 (Chinese Standard Time, CST). OC was determined using a DRI 2000A carbon analyzer (Desert Research Institute, Reno, NV, USA) following the IMPROVE protocol (Chow et al., 1993), and the concentrations of sulphate, nitrate and ammonium were determined by ion chromatography using an IC 3000 (Dionix Corp., Sunnyvale, CA, USA). Overall, the agreement of these comparisions was good, but the organics did not match well, with $r^2 = 0.40$.

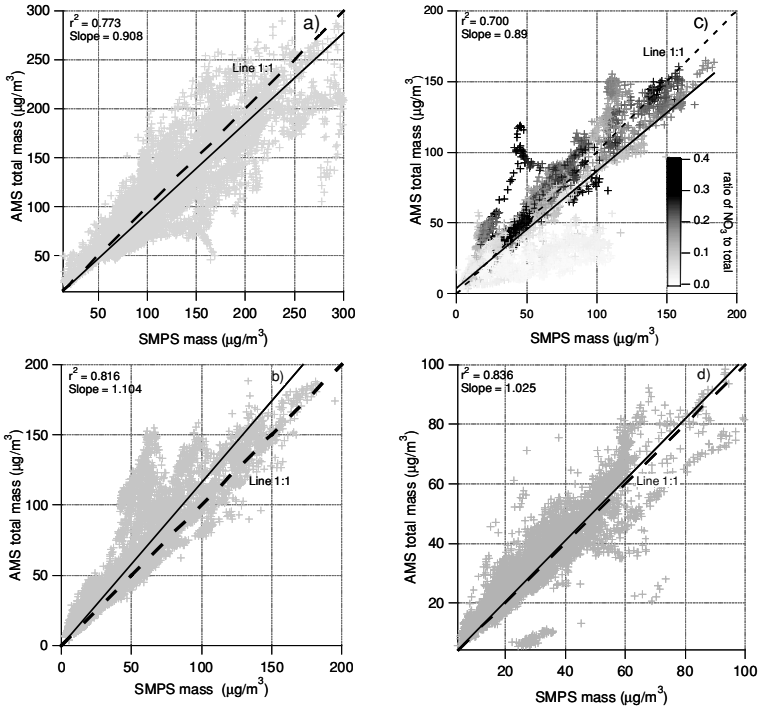

Fig. 1. Correlation plots of AMS-measured total mass concentrations versus SMPS-measured mass concentrations. The lines are linear fits to the data. Plot (a) is for June 2008; (b) is for July 2008; (c) is for August 2008; (d) is for September 2008. Note that in plot (c) the data are shaded on the basis of the contribution of nitrate to total mass.

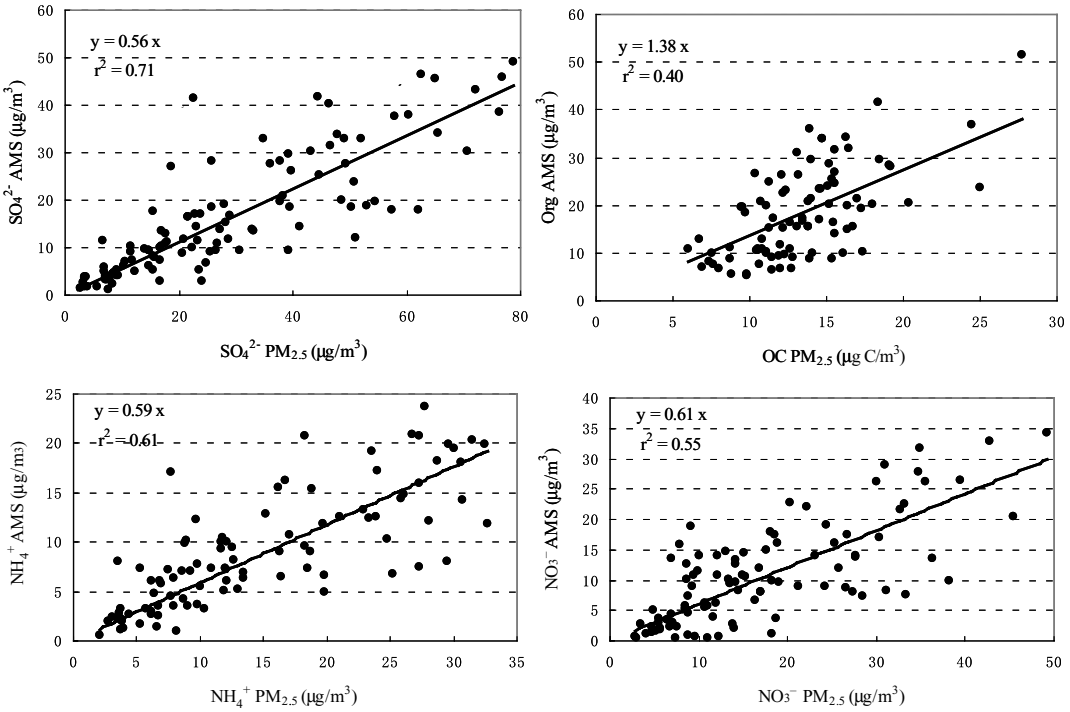

Fig. 2. Correlation plots of AMS-measured species versus chemical data $PM_{2.5}$ filter samples from 09:00 to 09:00 China Standard Time.

One possible reason for the lack of agreement in OC concentrations is that the type of organic aerosol can lead to an overestimation of primary organic aerosols and underestimation of the secondary (He et al., 2005). Along these lines, Jimenez et al. (2003) suggested that the relative ionization efficiency (RIE) of organic matter derived from combustion sources is generally larger than that for aerosols produced via the oxidation of organics. These differences in RIEs can result in an overestimation of small organic particles that are mainly from primary emission and an underestimation of the secondary organic aerosols, which are mostly in the accumulation mode. Another possible explanation is that some organic materials are lost from filters during the 24 h of sampling. The major ions in the filter samples matched reasonably well with the AMS data: the r^2 values for $SO_4^{2-} = 0.71$, $NO_3^- = 0.55$ and $NH_4^+ = 0.61$. Similar agreement between data collected with an AMS versus filter samples was reported for a study in Pittsburgh, PA, in the United States (He et al., 2005).

To better understand the chemical composition of the OA and sources for that material, the AMS mass spectra (MS) matrices for OA were analysed by Positive Matrix Factorization (PMF, Paatero and Tapper, 1994) as described by (Ulbrich et al., 2009). The mass concentrations and MS of three distinct components, including one hydrocarbon-like OA fraction (HOA) and two oxygenated OA fractions (OOA I and OOA II), were determined (Fig. 3). Components classified as HOA have been frequently observed in urban atmospheres (Zhang et al., 2005a, b; Lanz et al., 2007; Zhang et al., 2007; Ulbrich et al., 2009), and similarities in mass spectral pattern of this OA fraction and those of diesel vehicle exhaust and lubricating oil aerosols have been noted (Canagaratna et al., 2004). The MS of both OOA components showed features characteristic of oxidized organic material, that is, a major peak at m/z 44 (CO_2^+, Alfarra, 2004; Zhang et al., 2005a). Differences in the intensity of m/z 44 fragments, however, reflect the different levels of oxidation in these two OOA components. To be consistent with previous studies (Lanz et al., 2007; Ulbrich et al., 2009), the more oxidized component was referred to as OOA I while the less oxidized component was designated OOA II.

3. Results and discussion

3.1. NPF events

The NPF events during the study were identified based on the evolution of the size distributions and particle number concentrations following the definitions of Kulmala et al. (2004). More specifically, high number concentrations in both the nucleation and Aitken modes as well as obvious growth trends in these particle size classes were used to identify the NPF events. Particle growth rates (GRs) for these NPF events are calculated following the method described by Yue et al. (2010) and (Wiedensohler et al. (2009). Growth trends were modelled by cubic fitting of the relationship between the median diameter measured by SMPS during the growth interval and time: the resulting $\Delta D_p/\Delta t$ was defined as the GR for that time interval.

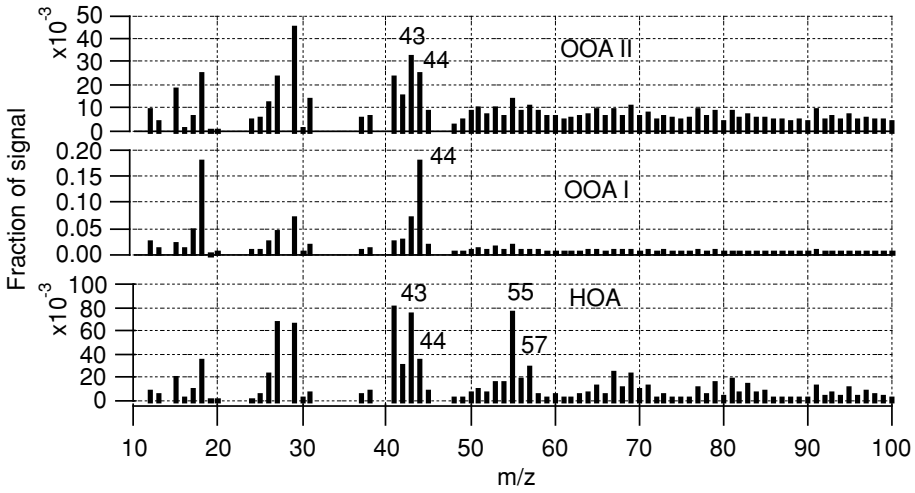

Fig. 3. The signal intensity of mass spectrum for three different types of organics. Hydrocarbon-like aerosol (HOA), more oxygenated organic aerosol (OOAI), less oxygenated organic aerosol (OOAII)

3.2. A case study of SA particle formation

Typically, NPF events in Beijing occured after periods in which the air was clean, and they were usually accompanied by relatively weak winds that changed in direction from northerly into southerly. Figure 4 presents the data collected during a typical NPF event. This episode began in the morning between ~08:00 to 09:00 CST on 17 July and continued till around 12:00. It followed elevated concentrations of the precursor-gases and featured a spike in the number of nucleation mode particles

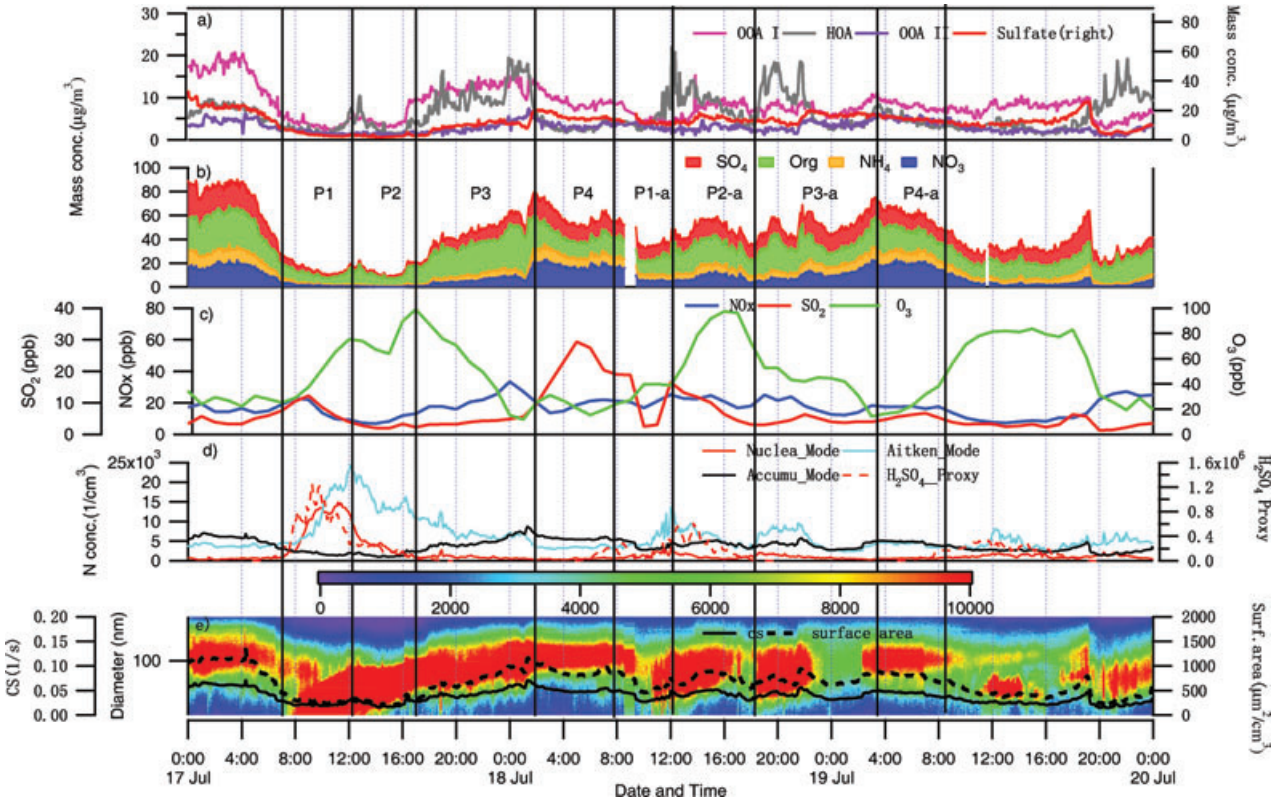

Fig. 4. Time series of (a) hydrocarbon-like aerosol (HOA), more oxygenated organic aerosol (OOAI), (b) less oxygenated organic aerosol (OOAII) in total organic matter, (c) aerosol concentrations, gases and O_3 concentrations, (d) number concentrations in different particle mode and H_2SO_4 proxy and (e) time series of aerosol particle size, condensational sink (CS) and surface area concentration.

($\sim 20 \times 10^3$ cm^{-3}) and ensuring growth in the Aitken mode. Simultaneous peaks for the sulphuric acid proxy and nucleation mode particles were seen in P1 as was an increase of surface O_3 and SO_2. Organic matter concentrations increased, but sulphate, nitrate and ammonium concentrations were at low levels and remained steady; low values for surface area and CS also were found. Relatively larger concentration increases were found for OOA I and HOA compared with OOA II and sulphate.

In Period 2 (P2) from 12:00 to 17:00 on 17 July, the O_3 concentration decreased and then rose to its maximum, presumably via photochemical reactions because the daily peak in solar radiation occurred during this period. Organics initially showed a downward trend and then their concentrations increased slightly; this was associated with a decrease in the number of nucleation mode particles, a relatively stable maximum size for the accumulation mode particles, and low values for surface area and CS.

From 17:00 to midnight (P3), the particles continued to grow, and the number concentration of particles in the accumulation mode increased especially sharply. Organics, sulphate, nitrate and ammonium products all showed increasing trends, but the concentrations of the organics were consistently higher than other SAs. The growth rate of total organics was 1.53 μg m^{-3} h^{-1} while that for OOA was 0.92 μg m^{-3} h^{-1} and that for sulphate was 0.64 μg m^{-3} h^{-1} (Table 1). The fact that the growth rate for organics was larger than that of sulphate implies that organics played a dominant role in SA formation even though sulphuric acid also contributed to the process. This result is consistent with other studies for the particle growth in Beijing (Zhang et al., 2004b). We also observed an inverse relationship between O_3 and organics from the beginning of this interval, that is, a decrease in O_3 but an increase in organics.

From 2:00 am to 9:00 am (P4) on the following day (18 July), high concentrations of a variety of precursor gases other than O_3 were observed; this presumably resulted from intensifying nighttime emissions of pollutants and a relatively shallow mixed layer. At the same time, high concentrations of all SA species were observed. Also on 18 July, and at roughly the same times as on the preceding day, a similar sequence of the four periods described (P1, P2, P3 and P4) was observed (Fig. 4). The trends in precursor gases and aerosols were generally consistent with those on the day before, and this suggests some recurring features in the formation of NPs and SA during the summer in Beijing.

3.3. Characteristics of 23 NPF events

We identified a total of 23 NPF episodes during the sampling campaign (Table 1), and these have been divided into five time intervals (I-1 to 5) on the basis of the types of pollution-control measures that were in place. During I-1 no special control measures were taken. From 1 to 19 July (I-2), about 300 000 'yellow-tag vehicles' were banned from the roads. These were highly polluting vehicles whose exhaust emissions exceeded the European Union Criteria I; examples include freight vehicles, tractors, low-speed cargo trucks, three-wheeled vehicles, motorcycles and vehicles used to transport hazardous chemicals. During I-3 motor vehicle traffic was reduced by alternately allowing only vehicles with even or odd license plates to operate, construction activities largely stopped, and coal power plant emissions were strictly limited. During the Beijing Olympic period (I-4, 8 to 24 August), additional measures were taken to further reduce coal-combustion emissions, and finally during the Paralympic Games period (25 August to 20 September, I-5), some of the control measures were eased (Zhang et al., 2009).

Time series plots of the size distributions, median diameter and fitted growth rates during five NPF events are presented in Fig. 5. The observed GRs from this study are generally smaller than those determined by (Yue et al., 2010) whose study also was conducted in Beijing. This difference in GRs can be explained by the fact that the 3–600 nm size range measured by Yue et al. was broader than in our study (12–550 nm). Consequently, more nucleation mode particles were measured in their study and that resulted in a larger growth rate. In addition, the two studies were conducted at different locations and therefore local differences probably also contributed to the discrepancies in GRs.

In the competition between NPF and condensation, nucleation is favoured by low particle surface areas, or more directly, by low CSs. This is clearly shown in our results (Table 1) because most of NPF episodes occurred when both particle surface area and CS were low. Strong northerly winds were often observed before NPF events: this is significant because winds from this direction sweep the aged aerosol away from Beijing as there are relatively few pollutant sources on that side of the city. Similarly, rainfall also often preceded NPF and this, too, would tend to cleanse the atmosphere and provide conditions that would support NPF. In the initial phase of a NPF event, a new particle mode ($<$25 nm) appeared, and it increased in particle number and was sustained for 2–3 h.

Chemically, the temporal variations in the sulphuric acid proxy (see Section 2, formula 1) and nucleation mode particles were quite similiar, indicating that the sulphuric acid played an important role in NPF (Fig. 6). This conclusion is consistant with the findings of (Yue et al., 2010) who also confirmed the dominant role of sulphuric acid in the nucleation processes. We cannot rule the role of OA in the NPF, however, because in the early stages of NPF, the OA concentrations often were high. As noted, only particles greater than 30 nm could be analysed with the AMS, and therefore the full size spectrum of nucleation mode particles could not be evaluated. Another limitation of our study is a lack of VOC (volatile organic component) data, and as a result of this, we do not have sufficient data to fully evaluate the importance of OA for NPF, but this will be investigated in our future work.

As noted, various measures were implemented during the 2008 Beijing Olympic Games to control air pollution, and these

Table 1. Summary of various indexed in 23 new particle formation (NPF) episodes from June–September in 2008

Interval ID	UFP formation duration time	Growth rate nm h^{-1}	OOA_GR ($\mu g\ m^{-3}\ h^{-1}$)	SO_4_GR ($\mu g\ m^{-3}\ h^{-1}$)	Wind direction	Precipitation before UFP	CS at NPF events (1/S)	Surface area ($\mu m^2\ cm^{-3}$)	Background PM1 conc. ($\mu g\ m^{-3}$)	SO_2 during growth period (ppb)	OOA in OM (%)
	6 June 09:15–10:25	8.06	1.00	1.35	NW-S	Y	0.015	258	19.7	5.4	–
I-1	8 June 10:45–13:35	8.32	1.66	1.50	NE-S	–	0.084	1440	97.2	12.9	59.6
	21June 08:20–10:00	8.64	2.89	2.62	N-S	–	0.035	601	42.0	9.0	–
	3 July 13:20–14:20	nd	nd	nd	NE-SW	–	0.018	280	39.0	3.9	–
	5 July 16:35–18:10	5.96	1.11	0.81	N-S	Y	0.015	244	10.9	3.1	–
	6 July 07:25–08:55	6.76	0.76	0.09	NE-SE	Y	0.028	512	23.8	2.4	–
I-2	10 July 18:20–20:10	13.90	2.49	4.79	NE-SE	–	0.042	897	30.2	4.2	58.6
	12 July 06:30–09:30	4.45	nd	nd	NE-S	–	0.025	265	47.7	3.5	–
	15 July 10:10–10:55	6.45	1.10	2.02	NE-S	Y	0.017	302	15.7	1.8	–
	16 July 10:10–11:10	5.69	1.62	2.41	N-S	–	0.041	674	30.0	7.5	–
	17 July 07:05–09:55	5.27	0.92	0.64	N-SE	–	0.021	296	11.0	2.7	–
	29 July 14:15–15:15	6.74	0.72	1.20	NE-SE	–	0.009	121	8.8	4.5	–
I-3	1 August 09:20–10:25	3.88	0.43	0.11	N-S	Y	0.010	215	10.7	nd	62
	2 August 08:35–09:10	2.94	0.24	−0.29	N-S	–	0.030	466	19.1	nd	–
	12 August 09:15–11:45	7.66	0.88	1.81	NE-SE	Y	0.009	142	14.0	3.3	–
	15 August 09:25–12:05	4.72	0.87	0.41	NE-SE	Y	0.009	147	6.0	2.2	–
	16 August 10:10–11:25	2.73	0.29	0.08	NE-SE	–	0.008	140	9.4	1.7	–
I-4	18 August 11:20–12:20	nd	0.80	1.31	NE-S	–	0.007	210	14.7	0.7	58.8
	22 August 09:35–12:25	2.43	0.34	−0.08	NE-S	–	0.014	249	18.8	nd	–
	23 August 09:30–11:55	6.30	0.78	0.16	N-S	–	0.021	274	12.4	3.9	–
	24 August 10:10–12:10	nd	0.86	2.56	NE-SE	–	0.014	290	6.9	5.4	–
I-5	10 September 09:05–12:05	4.99	0.28	0.22	N-S	–	0.006	112	10.2	1.3	55.6
	12 September 09:25–11:05	4.30	0.33	−0.35	N-SE	–	0.015	195	10.0	4.5	–

nd, no data; UFP, Ultra-fine particle; OOA_GR, Growth rate of oxygenated organic arosol; SO4_GR, Growth rate of sulphate; CS, condensational sink.

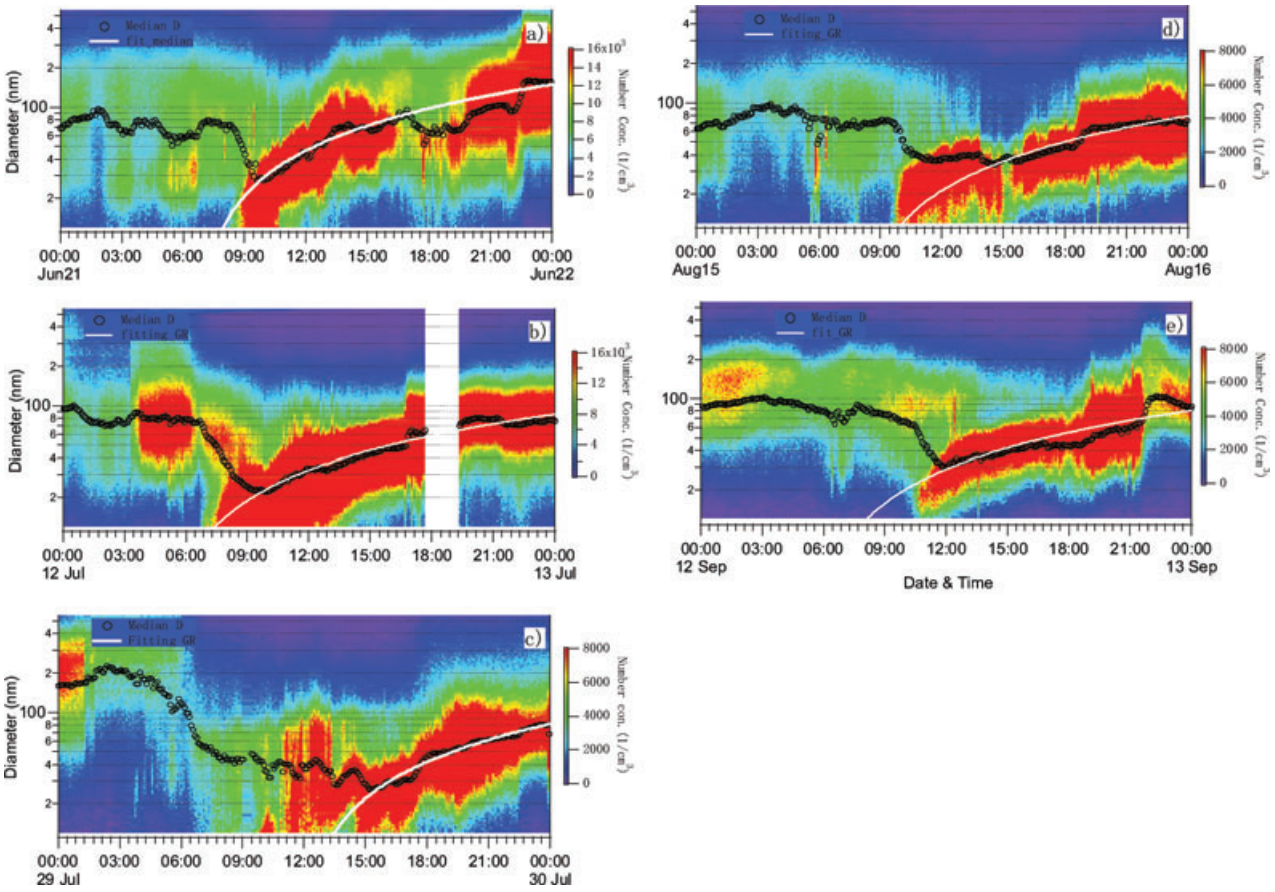

Fig. 5. The NPF events occurred during five time intervals (a–e correspond with intervals 1–5)

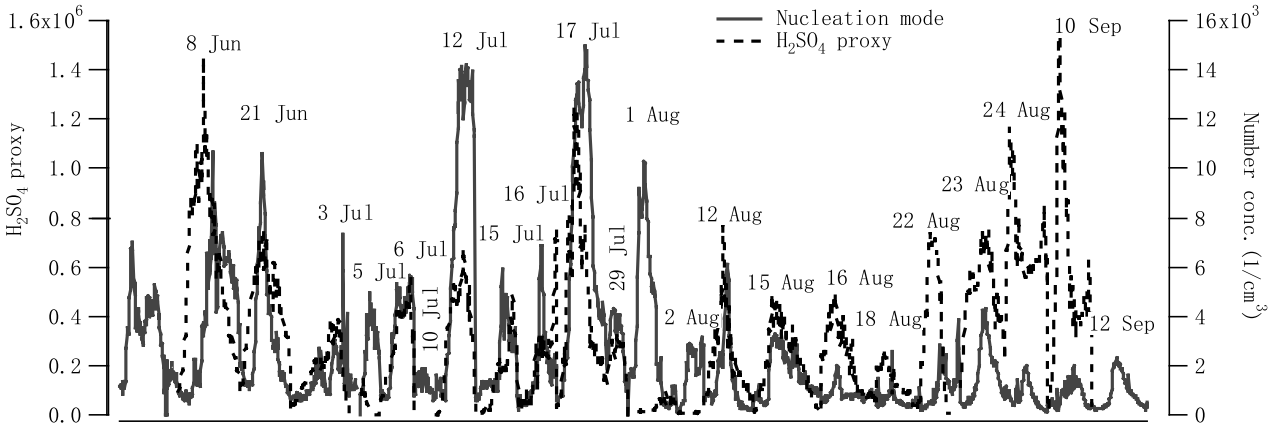

Fig. 6. Comparison between H_2SO_4 proxy and nucleation mode during NPF events.

measures apparently did affect particle formation. To facilitate the discussion of these effects, the study is divided into five time intervals, which are next discussed in sequence. During the first interval (I-1), which was before any special control measures had been implemented, relatively high particle concentrations (~93 μg m^{-3}) were observed, and the SO_2 concentration averaged 9.73 ppb (Table 1). This was higher than that during I-2 when the yellow-tagged vehicles were banned from roads. Three NPF events were observed during I-1, and the particle growth rates during that interval (8.06, 8.32 and 8.64 nm h^{-1}) were higher

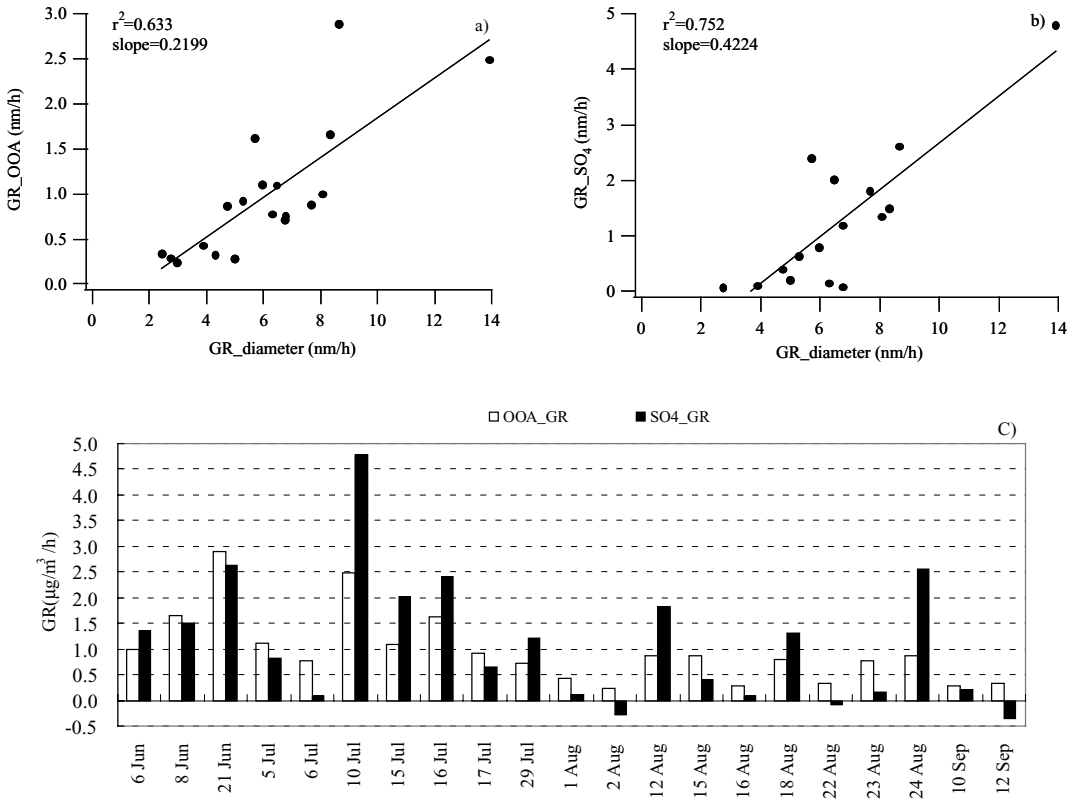

Fig. 7. Correlation between (a) growth rate of oxygenated organic aerosol and (b) sulphate versus diameter growth rate; (c) growth rates for OOA, sulphate in NPF events.

than in I-2. In I-3, when the measures were taken to limit motor vehicle traffic based on even versus odd license plates, the average SO_2 concentration dropped to 5.23 ppb, and the growth rate decreased to ∼4 nm h^{-1}. This suggests that the concentrations of precursor gases such as SO_2 affect the particles' growth rates. During the actual games, that is, I-4 (Olympic Games) and I-5 (Paralympic Games), the average concentrations of both PM and SO_2 remained at a rather low levels (∼30 to 40 μg m^{-3} for PM and 3–5 ppb for SO_2), and growth rates were slow.

To evaluate the contributions of organics and sulphuric acid to condensational growth, we plotted the particles' growth rates against those of OOA and sulphate (Figs 7a and b). It is obvious from these graphs that both the OOA and sulphate growth rates were strongly correlated with the particle growth, that is, the corresponding r^2 values for OOA_GR and SO_4_GR with the growth rate were statistically significant, 0.65 and 0.76, respectively (Figs 7a and b). This indicates that both organics and H_2SO_4 contributed to the growth processes, and this is also partially consistent with the Yue's model calculations that emphazied the role of H_2SO_4. The growth rates of OOA and sulphate for all 23 NPF events are plotted as time series, and one can see that there are only eight cases in which the SO_4_GR was greater

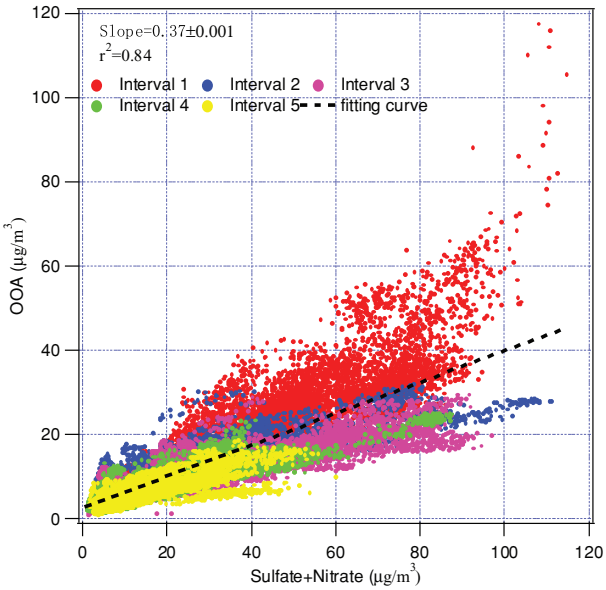

Fig. 8. Correlation between oxygenated organic aerosols (OOA, representing secondary organic carbon) and sulphate plus nitrate during the entire campaign (June–September 2008).

than the OOA_GR (Fig. 7c). This analysis thus shows that both organic and sulphur chemistry played major roles in particle growth.

3.4. *Role of organics and secondary organic aerosol in SA formation*

Among the more notable features of the data for the study were the relatively high concentrations and percentages of organic aerosols in PM_1 (20–80%). Even during the early stages of NPF formation, organics were the dominant aerosol species in the measured size range. Indeed, two of the organic fractions, OOA I and HOA, continued to the increase during the growth period, and their growth rates were larger than that of OOA II. Unfortunately, due to the inability of the AMS to detect the full size range of nucleation mode particles, we were not able to definitely evaluate the contribution of sulphate to the nucleation mode (Fig. 4).

Significant correlations between OOA (OOA I and OOA II) and the sum of sulphate and nitrate are a further indication that both organic and inorganic substances were involved the formation of the SAs (Fig. 8). Moreover, the particle formation processes involving these compounds were all likely influenced by common factors, especially weather (Zhang et al., 2009). As shown in Table 1, the oxygenated organic aerosol (OOA) composed ∼60% of the total organic mass through the entire observation period. This value is consistent with previous estimates made for a rural site in China (Zhang et al., 2005c), and at 14 Chinese sites (70% for rural and 60% for urban sites, Zhang et al., 2008). The relatively high proportions of OOA during I-1 when no special pollution control measures were in place and under stable weather conditions (Zhang

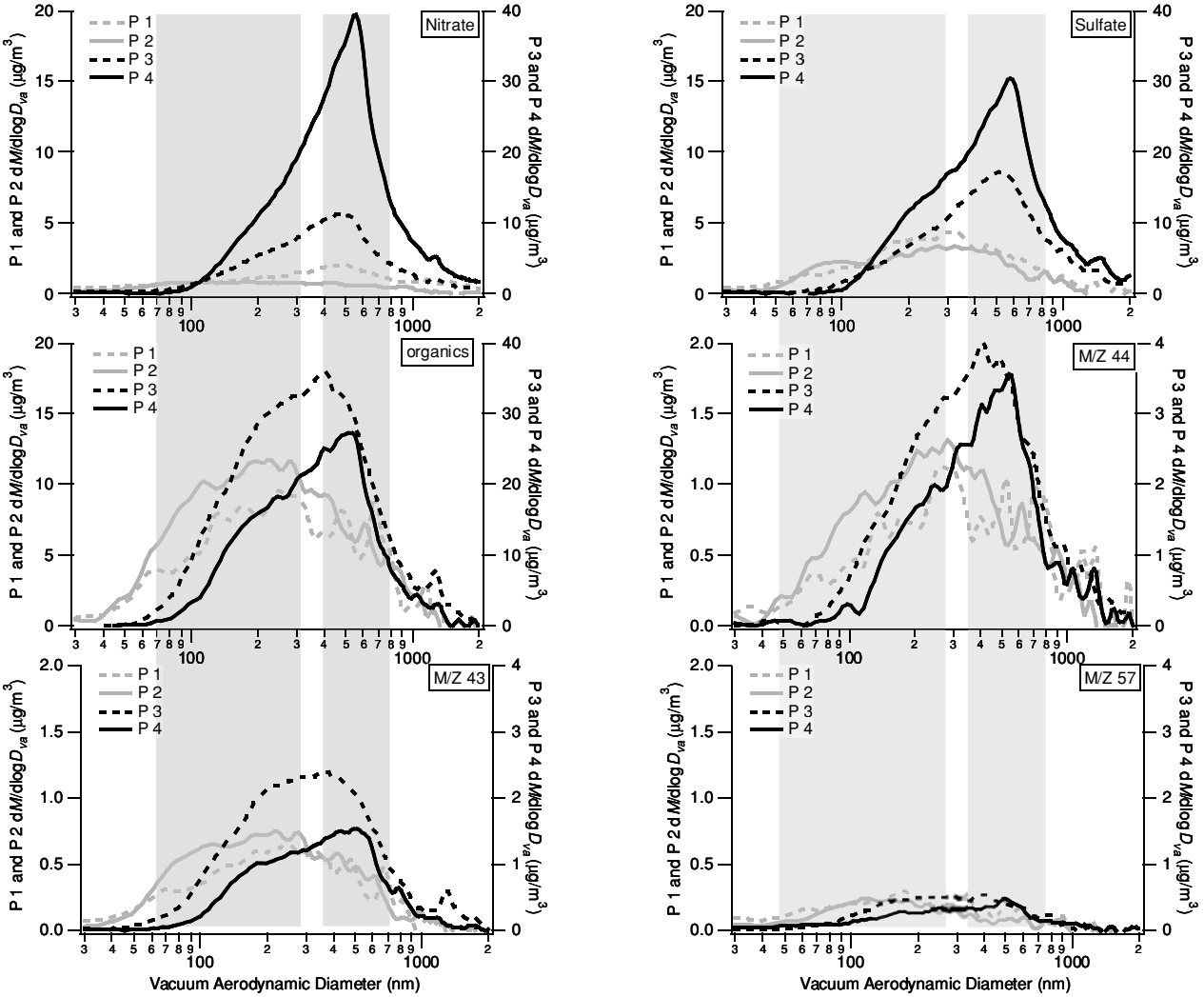

Fig. 9. Mass size distributions of nitrate, sulphate, organics and organic mass fragments (m/z 43, m/z 44, m/z 57) determined by AMS during four different periods (P1 to P4) during the NPF event on 17 July.

et al., 2009), suggested that a large quantity or high percentage OOA formed in polluted air masses and stable atmospheric conditions.

Plots of the mass-size distributions of nitrate, sulphate, organics and organic mass fragments (m/z 43, m/z 44, m/z 57) for the NPF event on 17 July (Fig. 9) show large peaks in particle diameters around 500 nm during the last two periods of SA formation (P3 and P4). This is an indication that submicron-sized particles produced via the gas-to-particle conversion of volatile organic compounds were a major contributor to the SA population. Unlike nitrate, the organics aerosols showed a bi-modal distribution during the early phases of SA formation (P1 and P2), with one peak around 100 nm and another around 200 nm. The first peak is characteristic of newly formed particles while the second peak is more representative of growing particles. Sulphate also showed bi-modal distribution, and although its bi-modality was less obvious than that of the organics, this is further evidence that sulphate also was involved in SA formation, including both nucleation and early particle growth. Organic species with m/z 43 and m/z 44 show trends in size distribution similar those of the total organics, suggesting an important role for OOA in both the nucleation and aging of organics. Notably, the m/z 57 signal, which is representive of HOA, remained at very low and steady concentrations during the various SA formation periods, suggesting a lesser involvement of HOA in SA formation.

4. Conclusions

NPF was investigated during a summertime sampling campaign in Beijing, and special attention was given to the formation of SA particles. Coordinated studies to measure changes in particle number/mass-size distributions during the nucleation, condensation and coagulation of aerosol particles were conducted to evaluate the effects of special pollution controls put in place for the Olympic games. One of the most noteworthy features in the entire campaign was the relative high concentrations and percentages (20–80%) of organic aerosols in the PM_1. Indeed, secondary organic aerosols accounted for ∼60% of the total organic aerosol.

Throughout the whole campaign, 23 NPF events were observed. Most of the NPF events started early in the morning when the winds were normally less than 4 m s^{-1} and there was a change in the wind direction from north to south. NPF events also tended to occur after precipitation events. The growth rates during the five stages of the NPF events apparently were influenced by types of pollution controls. When no controls were in place (I-1) or when yellow-tagged vehicles were banned (I-2), the average growth rates were 8.34 nm h^{-1} and 6.9 nm h^{-1}, respectively, while in contrast, during the Olympic Games, the average particle growth rates were reduced to 4.6 nm h^{-1}, presumably due to the combined effects of weather and the lower concentrations of precursor gases.

During the NPF events in Beijing, organic matter played an important role in the growth of particles. From an evaluation of the mass-size distributions for sulphate, nitrate, organics and tracers for HOA and OOA, it can be concluded that organics have a crucial contribution to early growth in SA formation. The organic species OOA tends to track the changes in total organics, suggesting its important role in the aging processes. The HOA fraction showed relatively low and invariable concentrations during the SA formation periods, suggesting relatively lesser involvement in SA formation.

5. Acknowledgments

This study was supported by grants from the National Basic Research Program of China (Grant No. 2011CB403401), the Aerosol-Precipitation Project of a Special Grant in Atmospheric Sciences Field supported by the CMA (GYHY200706036), the National Natural Science Foundation of China (Grant No. 40575063, 40705042), the China International Science and Technology Cooperation Project (2009DFA22800) and the Chinese Academy of Meteorological Sciences Foundation (Grant No. 2008Y004).

References

Alam, A. J., Shi, P. and Harrison, R. M. 2003. Observations of new particle formation in urban air. *J. Geophys. Res.* **108**(D3), 4093, doi:4010.1029/2001JD001417.

Alfarra, R. 2004. *Laboratory characterisation of the aerodyne aerosol mass spectrometer*, PhD Thesis, University of Manchester.

Allan, J. D., Bower, K. N., Coe, H., Boudries, H., Jayne, J. T. and co-authors. 2004. Submicron aerosol composition at Trinidad Head, California, during ITCT 2K2: its relationship with gas phase volatile organic carbon and assessment of instrument performance. *J. Geophys. Res.* **109**, D23S24, doi:10.1029/2003JD004208.

Canagaratna, M. R., Jayne, J. T., Ghertner, D. A., Herndon, S., Shi, Q. and co-authors. 2004. Chase studies of particulate emissions from in-use New York city vehicles. *Aerosol Sci. Technol.* **38**, 555–573.

Chow, J. C., Watson, J. G., Pritchett, L. C., Pierson, W. R., Frazier, C. A. and co-authors. 1993. The DRI thermal/optical reflectance carbon analysis system: description, evaluation and applications in U.S. air quality studies. *Atmos. Environ.* **27A**, 1185–1201.

Crosier, J., Allan, J. D., Coe, H., Bower, K. N., Formenti, P. and co-authors. 2007. Chemical composition of summertime Aerosol in the Po Valley (Italy), North Adriatic and Black Sea. *Q. J. R. Meterol. Soc.* **133**(S1), 61–75.

Dal Maso, M., Kulmala M., Lehtinen K. E. J., Mäkelä J. M., Aalto, P. and co-authors. 2002. Condensation and coagulation sinks and formation of nucleation mode particles in coastal and boreal forest boundary layers. *J. Geophys. Res.* **107**(D19), 8097, doi:8010.1029/2001JD001053.

Dal Maso, M. Kulmala, M., Riipinen, R., Wagner, T., Hussein, P. P. and co-authors. 2005. Formation and growth of fresh atmospheric aerosols: eight years of aerosol size distribution data from SMEAR II, Hyytiälä, Finland. *Boreal. Environ. Res.* **10**(5), 323–336.

Donaldson, K., Brown, D., Clouter, A., Duffin, R., MacNee, W. and co-authors. 2002. The pulmonary toxicology of ultrafine particles. *J. Aerosol Med.* **15**, 213–220.

Dunn, M. J., Jimenez, J. L., Baumgardner, D., Castro, T., McMurry, P. H. and co-authors. 2004. Measurements of Mexico City nanoparticle size distributions: observations of new particle formation and growth. *Geophys. Res. Lett.* **31**, L10102, doi:10.1029/2004GL019483.

Eisele, F. L. and McMurry, P. H. 1997. Recent progress in understanding particle nucleation and growth. *Phil. Trans. R. Soc. London, Ser.* **352**, 191–200.

Hämeri, K., Kulmala, M., Aalto, P., Leszczynski, K., Visuri, R. and co-authors. 1996. The investigations of aerosol particle formation in urban background area of Helsinki. *Atmos. Res.* **41**(3–4), 281–298.

He, L. Y., Hu, M., Feng, H. X. and Zhang, Y. H. 2005. Determination of organic molecular tracers in PM215 in the atmosphere of Beijing(in chinese). *Acta Scientice Circumstantiae* **25**(1), 23–29.

Jayne, J T., Leard, D.C., Zhang, X., Davidovits, P., Smith, K. A. and co-authors. 2000. Development of an aerosol mass spectrometer for size and composition analysis of submicron particles. *Aerosol Sci. Technol.* **33**, 49–70.

Jimenez, J. L., Jayne, J. T., Shi, Q., Kolb, C. E., Worsnop, D. R. and co-authors. 2003. Ambient aerosol sampling using the aerodyne aerosol mass spectrometer. *J. Geophys. Res.* **108**(D7), 8425, doi:8410.1029/2001JD001213.

Kulmala, M., Toivonen, A., Makela, J. M. and Laaksonen, A. 1998. Analysis of the growth of nucleation mode particles observed in Boreal forest. *Tellus Ser. B* **50**, 449–462.

Kulmala, M., Hämeri, K., Aalto, P. P., Makela, J. M., Pirjola, L. and co-authors. 2001. Overview of the international project on biogenic aerosol formation in the boreal forest (BIOFOR). *Tellus. Ser. B* **53**, 324–343.

Kulmala, M., Vehkamaki, H., Petäjä, T., Maso, M. D., Lauri, A. and co-authors. 2004. Formation and growth rates of ultrafine atmospheric particles: a review of observations. *J. Aerosol. Sci.* **35**(2), 143–176.

Kulmala, M., Petäjä, T., Mönkkönen, P., Koponen, I. K., Maso, M. D. and co-authors. 2005. On the growth of nucleation mode particles: source rates of condensable vapor in polluted and clean environments. *Atmos. Chem. Phys.* **5**, 409–416.

Lanz, V. A., Alfarra, M. R., Baltensperger, U., Buchmann, B., Hueglin, C. and co-authors. 2007. Source apportionment of submicron organic aerosols at an urban site by factor analytical modelling of aerosol mass spectra. *Atmos. Chem. Phys.* **7**, 1503–1522.

Li, N., Sioutas, C., Cho, A., Schmitz, D., Misra, C. and co-authors. 2003. Ultrafine particulate pollutants Induce oxidative stress and mitochondrial damage. *Environ. Health Perspect.* **111**, 455–460.

Lin, W., Xu, X., Zhang, X. and Tang, J. 2009. Contributions of pollutants from North China Plain to surface ozone at the Shangdianzi GAWStation. *Atmos. Chem. Phys.* **8**, 5889–5898.

Massling, A., Stock, M., Wehner, B., Wu, Z. J., Hu, M. and co-authors. 2008. Size segregated water uptake of the urban submicrometer aerosol in Beijing. *Atmos. Environ.* **43**, 1578–1589.

Matthew, B. M., Middlebrook, A. M. and Onasch, T. B. 2008. Collection efficiencies in an aerodyne aerosol mass spectrometer as a function of particle phase for laboratory generated aerosols. *Aerosol Sci. Technol.* **42**(11), 884–898.

Mönkkönen, P., Koponen, I. K., Lehtinen, K. E. J., Hameri, K., Uma, R. and co-authors. 2005. Measurements in a highly polluted Asian mega city: observations of aerosol number size distribution, modal parameters and nucleation events. *Atmos. Chem. Phys.* **5**, 57–66.

O'Dowd, C. D., Geever, M., Hill, M. K., Smith, M. H. and Jennings, S. G. 1998. New particle formation: spatial scales and nucleation rates in the coastal environment. *Geophys. Res. Lett.* **25**, 1661–1664.

O'Dowd, C. D., Bahreini, R., Flagan, R.C., Seinfeld, J. H., Hameri, K. and co-authors. 2002. Marine aerosol formation from biogenic iodine emissions. *Nature* **417**, 632–636.

Oberdörster, G., Celein, R. M., Ferin, J. and Weiss, B. 1995. Association of particulate air pollution and acute mortality: involvement of ultrafine particles? *Inhal. Toxicol.* **7**(1), 111–124

Paatero, P. and Tapper, U. 1994. Positive matrix factorization: a nonnegative factor model with optimal utilization of error estimates of data values. *Environmetrics* **5**, 111–126.

Pirjola, L., Laaksonen, A., Aalo, P. and Kulmala, M. 1998. Sulfate aerosol formation in the Arctic boundary layer. *J. Geophys. Res.-Atmos.* **103**, 8309–8321.

Quinn, P. K., Bates, T. S., Coffman, D., Onasch, T. B., Worsnop, D. R. and co-authors. 2006. Impactors of sources ang aging on submicronmeter aerosol properties in the marine boundary layer across the Gulf of Marine. *J. Geophys. Res. -Atmos.* **111**, D23S36, doi:10.1029/2006JD007582.

Sun, J. Y., Zhang, Q., Canagaratna, M. R., Zhang, Y. M., Ng, N. L. and co-authors. 2010. Highly time- and size-resolved characterization of submicron aerosol particles in Beijing using an aerodyne aerosol mass spectrometer. *Atmos. Environ.* **2010**(44), 131–140.

Tobias, H. J., Kooiman, P. M., Docherty, K. S. and Ziemann, P. J. 2000. Real-time chemical analysis of organics aerosols using a thermal desorption particle beam mass spectrometer. *Aerosol Sci. Technol.* **33**(1–2), 170–190.

Ulbrich, I. M., Canagaratna, M. R., Zhang, Q., Worsnop, D. R. and Jimenez, J. L. 2009. Interpretation of organic components from positive matrix factorization of aerosol mass spectrometric data. *Atmos. Chem. Phys.* **9**, 2891–2918.

Weber, R. J., McMurry, P. H., Mauldin, R. L., Tanner, D. J., Eisele, F. L. and co-authors. 1999. New particle formation in the remote troposphere: a comparison of observations at various sites. *Geophys. Res. Lett.* **26**, 307–310.

Wehner, B., Wiedensohler, A., Tuch, T. M., Wu, Z. J., Hu, M. and co-authors. 2004. Variability of the aerosol number size distribution in Beijing, China: new particle formation, dust storms, and high continental background. *Geophys. Res. Lett.* **31**, L22108, doi:22110.21029/22004GL021596.

Wiedensohler, A., Wehner, B. and Birmili, W. 2002. Aerosol number concentrations and size distributions at mountain-rural, urban-influenced rural, and urban-background sites in Germany. *J. Aerosol. Med.* **15**, 237–243.

Wiedensohler, A., Cheng, Y. F., Nowak, A., Wehner, B., Achtert, P. and co-authors. 2009. Rapid aerosol particle growth and increase of cloud condensation nucleus activity bysecondary aerosol formation and condensation: a case study for regional air pollution in northeastern China. *J. Geophys. Res.-Atmos.* **114**, D00G08. doi:10.1029/2008JD010884.

Wu, Z., Hu, M., Liu, S., Wehner, B., Bauer, S. and co-authors. 2007. New particle formation in Beijing, China: statistical analysis of a 1-year data set. *J. Geophys. Res.-Atmos.* **112**, D09209, doi:09210.01029/02006JD007406.

Xu, X., Lin, W.,Wang, T., Yan, P., Tang, J. and co-authors. 2008. Long-term trend of surface ozone at a regional background station in eastern China 1991–2006: enhanced variability. *Atmos. Chem. Phys.* **8**, 2595–2607.

Yue, D. L., Hu, M., Zhang, R. Y., Wang, Z. B., Zheng, J. and co-authors. 2010. The roles of sulfuric acid in new particle formation and growth in the mega-city of Beijing. *Atmos. Chem. Phys.* **10**, 4953–4960.

Zhang, Q., Stanier, C. O., Canagaratna, M. R., Jayne, J. T., Worsnop, D. R. and co-authors. 2004a. Insights into the chemistry of new particle formation and growth events in Pittsburgh based on Aerosol Mass Spectrometry. *Environ. Sci. Technol.* **38**, 4797–4809.

Zhang, R. Y., Suh, I., Zhao, J., Zhang, D., Fortner, E. C. and co-authors. 2004b. Atmospheric new particle formation enhanced by organic acids. *Science* **304**, 1487–1490.

Zhang, Q., Alfarra, M. R., Worsnop, D. R., Allan, J. D., Coe, H. and co-authors. 2005a. Deconvolution and quantification of hydrocarbon-like and oxygenated organic aerosols based on aerosol mass spectrometry. *Environ. Sci. Technol.* **39**(13), 4938–4952.

Zhang, Q., Worsnop, D. R., Canagaratna, M. R. and Jimenez, J. L. 2005b. Hydrocarbon-like and oxygenated organic aerosols in Pittsburgh: insights into sources and processes of organic aerosols. *Atmos. Chem. Phys.* **5**, 3289–3311.

Zhang, X. Y., Wang, Y. Q., Wang, D. and Gong, S. L. 2005c. Characterization and sources of regional-scale transported carbonaceous and dust aerosols from different pathways in costal and sandy land areas of China. *J. Geophys. Res.* **110**, D15301, doi:15310.11029/12004JD005457.

Zhang, Q., Jimenez, J. L., Canagaratna, M. R., Allan, J. D., Coe, H. and co-authors. 2007. Ubiquity and dominance of oxygenated species in organic Aerosols in anthropogenically-influenced Northern Hemisphere mid-latitudes. *Geophys. Res. Lett.* **34**, L13801, doi:13810.11029/12007GL029979.

Zhang, X. Y., Wang, Y. Q., Zhang, X. C., Guo, W. and Gong, S. L. 2008. Carbonaceous aerosol composition over various regions of China during 2006. *J. Geophys. Res.* **113**, D14111, doi:14110.11029/12007JD009525.

Zhang, X. Y., Wang, Y. Q., Lin, W. L., Zhang, Y. M., Zhang, X. C. and co-authors. 2009. Changes of atmospheric compositions and optical property over Beijing: 2008 Olympic Monitoring Campaign. *Bull. Am. Meteorol. Soc.* **90**, 1633–1651.